Journal of Materials Chemistry A

ROYAL SOCIETY OF CHEMISTRY

PAPER

View Article Online
View Journal | View Issue

Cite this: J. Mater. Chem. A, 2022, 10, 12055

Novel membranes with extremely high permeability fabricated by 3D printing and nickel coating for oil/water separation†

Lei Han, Cheng Chen, Liguo Shen, * Hongjun Lin, * Bisheng Li, Zhengyi Huang, Yanchao Xu, Renjie Li and Huachang Hong

Traditional membranes for oil/water separation are subjected to the severe mutual constraint between selectivity and permeability. Fabricating membranes with extremely high permeance as well as high separation efficiency is an eternal pursuit of the research community. This study provides a robust strategy to achieve this goal. In the current study, a novel acrylonitrile–butadiene–styrene–nickel (ABS-Ni) membrane for oil/water separation was firstly developed by three-dimensional (3D) printing technology followed by *in situ* Ni coating. A series of characterization results demonstrate that the novel ABS-Ni membrane was successfully fabricated. The prepared ABS-Ni membrane showed underwater superoleophobicity, verified by its oil contact angle of 151.96°. The antifouling tests and extended Derjaguin–Landau–Verwey–Overbeek (XDLVO) theory reveal that the ABS-Ni membrane had a preferable antifouling surface. The filtration tests show that the ABS-Ni membrane possessed more than 99% oil rejection to 5 typical oil/water systems, namely *n*-hexane, soybean oil, gasoline, diesel and petroleum ether. Meanwhile, the flux of the ABS-Ni membrane reached as high as 5.34×10^4 L m^{-2} h^{-1}, outperforming all of the state-of-the-art membranes for oil/water separation to our knowledge. Moreover, both the flux and separation efficiency could remain above 99% after 10 cycling filtration processes, and the ABS-Ni membrane maintained stable separation functionality within a pH range from 1 to 13. This work presents a robust membrane with extremely high permeability as well as a novel membrane fabrication method for oil/water separation.

Received 12th March 2022
Accepted 4th May 2022

DOI: 10.1039/d2ta01971j

rsc.li/materials-a

1. Introduction

Being a typical pressure-driven membrane separation process, oil/water separation has become one of the hottest topics in the fields of environmental protection and chemical industry all over the world.[1] Increasing untreated oily wastewater discharge and frequent oil spill accidents are causing serious environmental problems.[2–5] Traditional treatment approaches, including coagulation,[6] air flotation,[7] and oil-absorbing materials,[8] are usually accompanied with the inherent problems of high energy consumption, low efficiency, tedious operation process and secondary contamination, limiting their wider applications. Among the various oily wastewater treatment approaches, membrane technology has been demonstrated to be very efficient for oil/water separation while simultaneously avoiding the above-mentioned problems to a great extent,[9–13] showing fantastic application prospects. However, the membranes used for oil/water separation are generally fabricated by phase inversion-based methods, which are associated with abundant solvent consumption, air and water pollution, and the inability to design the membrane structure and pore size.[1,14] Meanwhile, for membrane technology itself, membrane fouling and the trade-off effect between permeability and selectivity are still big challenges severely limiting its industrial applications.[15–18] Fabricating membranes with extremely high permeance but high separation efficiency is an eternal pursuit of the research community. Therefore, developing solvent-free membrane fabrication methods and improving membrane performance are both indispensable for efficient oil/water separation.

Three-dimensional (3D) printing has brought great benefits to a wide range of industries since its inception in the mid-1980s.[19] For 3D printing, acrylonitrile–butadiene–styrene (ABS) is one of the most common materials due to its stability, good tensile strength, high bending resistance, environmental friendliness and low cost.[20–22] Since 3D printing enables the fabrication of complicated objects with almost no geometrical constraints,[23] it is possible to use this solvent-free method to fabricate polymeric membranes. Moreover, 3D printing is based on the sequential layer-by-layer deposition of the material, and is a highly customizable technology.[23] This means that the

College of Geography and Environmental Sciences, Zhejiang Normal University, Jinhua, China, 321004. E-mail: lgshen@zjnu.cn; hjlin@zjnu.cn

† Electronic supplementary information (ESI) available. See https://doi.org/10.1039/d2ta01971j

membrane structure and pore size can be designed, allowing us to significantly reduce membrane fouling and the trade-off effect when the fabricated membrane is used. It is therefore anticipated that fabricating membranes by 3D printing technology will overcome the above-mentioned problems in the process of oil/water separation.

Despite the great potential, studies regarding the fabrication of polymeric membranes for oil/water separation by 3D printing are still quite limited. By reviewing the related studies, it is found that they mainly focus on the fabrication of spacers,[24,25] other modules[26,27] and ceramic membranes.[28] From these limited studies, the benefits of adopting 3D printing have been well evidenced. For instance, it was reported that mass transfer in a 3D printed contactor was much higher than in hollow fiber membranes.[29] The membrane fabricated by the deposition of a thin polyethersulfone (PES) selective layer over a 3D printed wavy support showed a high oil rejection of 96% ± 3% but low permeance for oil/water separation.[30] The situation of limited research may be due to the insufficient resolution of 3D printing[19] and the high fouling propensity of ABS,[31,32] the most popular polymeric material used in 3D printing. It is known that nickel is a stable and cheap metal. Ni coating can make the ABS surface metallized, which can improve the membrane's hydrophilicity, corrosion resistance, acid and alkali resistance and other properties. Recently, the deposition of a nickel (Ni) layer on a membrane support has been used to improve membrane performance. It was reported that a Ni-layer-based conductive membrane combined with an external electric field showed complete rejection of Congo red and significantly improved permeance.[33] Inspired by these studies, it is hypothesized that depositing a Ni layer on a 3D printed ABS support will mitigate the fouling propensity of the ABS support and endow the membrane with many good properties, thus accelerating the practical process of 3D printing for oil/water separation. To our knowledge, no one has tested this hypothesis to date.

Herein, for the first time, a novel ABS-Ni membrane was successfully developed by 3D printing technology for oil/water separation. The prepared ABS-Ni membrane displayed excellent hydrophilic and superoleophobic ability, resulting into 99% oil rejection for 5 typical sample systems. A high flux of 5.34×10^4 L m^{-2} h^{-1}, excellent antifouling ability and stability were also obtained. This work represents a timely contribution that would be of interest to the broad academic community concerned with membrane technology for oil/water separation.

2. Materials and methods

2.1. Materials

Acrylonitrile–butadiene–styrene (ABS) was provided by Stratasys. Silver nitrate ($AgNO_3$), dimethylaminoborane ($C_2H_{10}BN$), potassium permanganate ($KMnO_4$), sodium pyrophosphate ($Na_4P_2O_7 \cdot 10H_2O$), sodium phosphate (Na_3PO_4), sodium carbonate (Na_2CO_3), concentrated sulfuric acid (H_2SO_4) and ammonia (NH_3 H_2O, 28%) were purchased from Sinopharm Chemical Reagent Co., Ltd, Meryer (Shanghai) Chemical Technology Co., Ltd Phosphoric acid (H_3PO_4) was supplied by Shanghai Lianshi Chemical Reagent Co., Ltd All the chemicals were used without pretreatment.

2.2. ABS-Ni membrane preparation

Fig. 1 shows a schematic of the preparation process of the ABS-Ni membranes. Firstly, models of the membranes were designed using the 3Dmax software, and then imported into the Grab CAD software to send instructions to industrial-grade 3D printers (F270, Stratasys, USA). The ABS membrane was printed by a 3D printer and subjected to an alkaline degreasing treatment. Thereafter, the ABS membrane was coated with Ni *via* an *in situ* reduction method. In detail, the pretreated ABS membrane was dipped in a silver nitrate solution (1.597 g L^{-1}) for 40 min at 25 °C to absorb silver ions (Ag^+). Meanwhile, 25 g $NiSO_4 \cdot 6H_2O$, 50 g $Na_4P_2O_7 \cdot 10H_2O$, 45 mL NH_3 H_2O and 1.5 g $C_2H_{10}BN$ were added sequentially to a flask with 1 L pure water to carry out the reduction reaction.[33] The membranes were fabricated in the following reaction conditions: temperature of 25 °C and duration of 4 min.

2.3. Characterization

A contact angle measuring instrument (Kino Co., Ltd, USA) was used to measure the contact angle of water on the membrane surface. The surface morphology of the membrane was characterized by scanning electron microscopy (SEM, LEO 1530VP, Germany) and optical microscopy (BX43, OLYMPUS, Japan). The functional groups on the membrane sample surface were investigated using a NEXUS 670 infrared spectrometer. X-ray photoelectron spectroscopy (XPS) (Thermo Fisher Scientific, ESCALAB 250Xi, USA) was applied to determine the chemical composition. An A1k X-ray was used as the excitation source in all the tests. X-ray diffractometry (XRD, Bruker D8 ADVANCE, Germany) with a test range from 20° to 80° (40 mA and 40 kV) was applied to characterize the samples. The zeta potential of each sample was determined by a Malvern Zetasizer Nano ZS instrument. The detailed methods can be found in the literature.[21,34–37]

2.4. Membrane performance tests

The membrane was embedded into a tube device with 1.78 cm^2 effective separation area. The organic solvent and water (dyed with methylene blue and oil red O, respectively) were mixed at a volume ratio of 1 : 1. Only gravity was used to drive the separation process where an oil/water mixture was directly

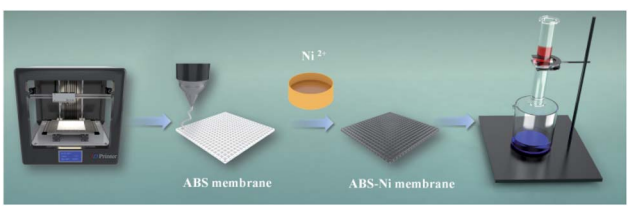

Fig. 1 A preparation schematic of the ABS-Ni membranes *via* 3D printing technology.

poured onto the membrane's upper surface.[38,39] The separation efficiency can be evaluated by eqn (1):

$$\text{Separation efficiency}(\%) = \frac{m_1}{m_0} \times 100 \quad (1)$$

where m_1 and m_0 represent the mass of the permeated oil and the oil before separation, respectively.

The oil permeation flux J (L m^{-2} h^{-1}) can be calculated according to eqn (2):

$$J = \frac{V}{A \times t} \quad (2)$$

where V, A and t represent the permeated oil volume (L), effective membrane area (m^2) and permeation time (h), respectively.

2.5. XDLVO approach

In order to explore the antifouling mechanism, XDLVO theory was employed to evaluate the acid–base forces, electrostatic forces and van der Waals forces at the interface.[40,41] The interaction energies at a separation distance h are represented by $\Delta G^{AB}(h)$, $\Delta G^{EL}(h)$ and $\Delta G^{LW}(h)$, respectively,[42] as shown by the following equations:

$$\Delta G_{h_0}^{AB} = 2\left[\sqrt{\gamma_w^+}\left(\sqrt{\gamma_f^-} + \sqrt{\gamma_m^-} - \sqrt{\gamma_w^-}\right) + \sqrt{\gamma_w^-}\left(\sqrt{\gamma_f^+} + \sqrt{\gamma_m^+} - \sqrt{\gamma_w^+}\right) - \sqrt{\gamma_f^-\gamma_m^+} - \sqrt{\gamma_f^+\gamma_m^-}\right] \quad (3)$$

$$\Delta G_{h_0}^{EL} = \frac{\mathscr{E}_0\mathscr{E}_r\kappa}{2}\left(\xi_f^2 + \xi_m^2\right)\left[1 - \coth(\kappa h_0) + \frac{2\xi_f\xi_m}{\xi_f^2 + \xi_m^2}\operatorname{csch}(\kappa h_0)\right] \quad (4)$$

$$\Delta G_{h_0}^{LW} = -2\left(\sqrt{\gamma_m^{LW}} - \sqrt{\gamma_w^{LW}}\right)\left(\sqrt{\gamma_f^{LW}} - \sqrt{\gamma_w^{LW}}\right) \quad (5)$$

where γ^{LW}, $\gamma^+$and γ^- are the LW surface tension, and electron donor and electron acceptor component, respectively; w, f and m stand for water, pollutant and membrane, respectively. The surface tension was obtained by calculation based on the contact angle values.[34,43,44]

3. Results and discussion

3.1. Optimal membrane selection

As shown in Fig. 2, ABS membranes with different pore sizes have been successfully prepared by 3D printing technology. From Fig. 2I, it can be seen that the ABS membranes are interlaced with two layers of ABS filaments, which form rectangular pores. Fig. 2II shows the morphology of the modified ABS-Ni membranes. In the modification process, the metal nickel layer was covered onto the ABS plastic filaments; therefore, it can be seen from the images that the rectangular pores are present between the dark filaments. Furthermore, due to the large pore size of the ABS membrane, the deposition of a metallic nickel layer on the membrane surface has minor effects on the membrane pore size.

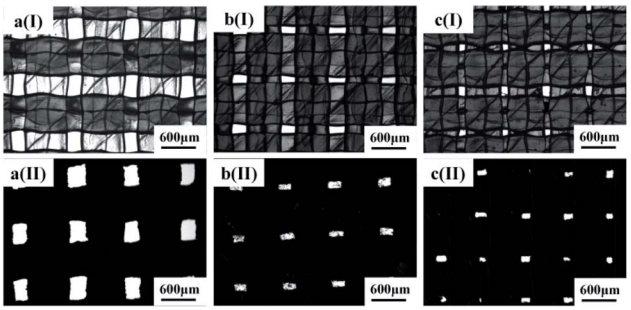

Fig. 2 Microscopic images of the prepared membranes with different pore sizes ((a), 240 × 400 μm, (b), 100 × 240 μm, (c), 100 × 150 μm; I represents ABS membranes; II represents ABS-Ni membranes).

Flux and separation efficiency analysis tests were carried out for the modified membranes with different pore sizes to select the optimal membrane. The experimental results in Fig. 3 indicate that the flux of the modified ABS-Ni membrane is not significantly decreased but is in fact promoted in comparison with that of the bare ABS membrane (Fig. 3a). This can be attributed to the fact that under the premise of basically no difference in pore size, the use of metallic nickel to modify the original membrane greatly improved the roughness and hydrophilicity of the membrane. Therefore, the flux of the modified membrane was much higher than that of the original membrane. Subsequent oil/water separation experiments show that the separation efficiency of the bare membrane is 0% regardless of the pore size, indicating that the bare membrane cannot be used for oil/water separation, while the ABS-Ni membrane with a pore size dimension of 240 μm × 400 μm displays more than 80% separation efficiency for the oil/water mixture. Moreover, the separation efficiency of the modified ABS-Ni membrane with a pore size dimension of 100 μm × 150 μm reaches 99.78% (Fig. 3b), with an extremely high flux of 53 366 L m^{-2} h^{-1}. Therefore, the modified membrane with a pore size dimension of 100 μm × 150 μm presents the optimal performance and was selected for all the following experiments.

3.2. Characterization

Optical images of the ABS and ABS-Ni membranes are shown in Fig. 4. The bare membrane exhibits an opaque ivory color, while the ABS-Ni membrane presents a silvery metallic luster, which can confirm the successful coating of a nickel layer on the ABS surface. The surface and cross-sectional SEM morphologies (Fig. 4h) further show that the ABS-Ni membranes have been

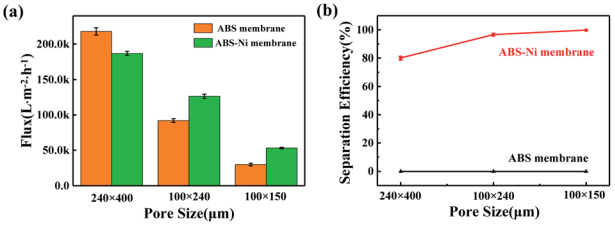

Fig. 3 Flux and separation efficiency of ABS and ABS-Ni membranes with different pore sizes.

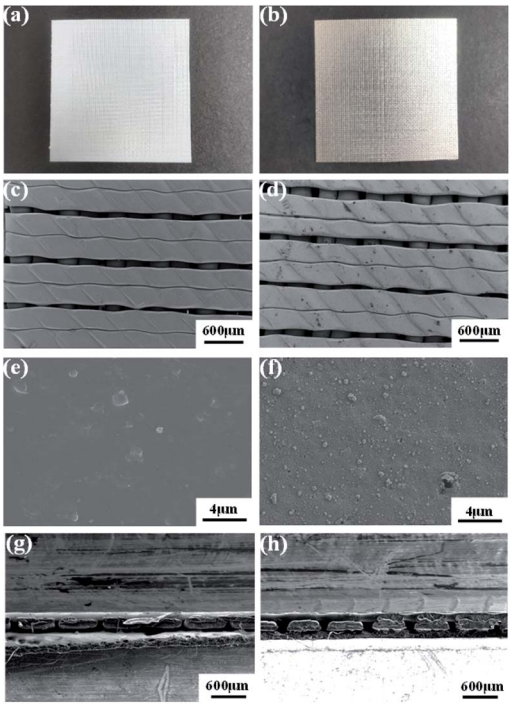

Fig. 4 Pictures and SEM images of the ABS and ABS-Ni membranes (left column represents ABS membranes, right column represents ABS-Ni membranes).

successfully obtained.[45,46] It is evident that a thin Ni layer is evenly coated on the 3D ABS frame. Compared with the smoother bare membrane, the successful coverage of nickel particles greatly improves the roughness of the modified membrane.

Fig. 5 gives the underwater oil contact angle (UOCA) and water contact angle (WCA) of the bare and the modified membranes. The ABS membrane is hydrophobic but oleophilic with poor oil resistance ability. After the nickel layer is plated on the membrane surface, the WCA of the membrane decreases from 96.87° (ABS membrane) to 30.84° (ABS-Ni membrane). Moreover, the UOCA increases from 37.86° (ABS membrane) to 151.96° (ABS-Ni membrane), which indicates that the ABS-Ni membrane possesses an underwater superoleophobic property.

As shown in Fig. 6a, the XRD spectra have a wide peak at about 20° that represents the amorphous nature of ABS. The peak at 44.5° can be attributed to the characteristic lattice (1, 1, 1) of Ni in the ABS-Ni membrane. The energy dispersive X-ray spectroscopy (EDS) mapping results also confirm that the nickel elements are coated onto the ABS surface, as shown in Fig. 6c. From Fig. 6, it is also confirmed that the Ni coating layer is rather thin and has a relatively even distribution.

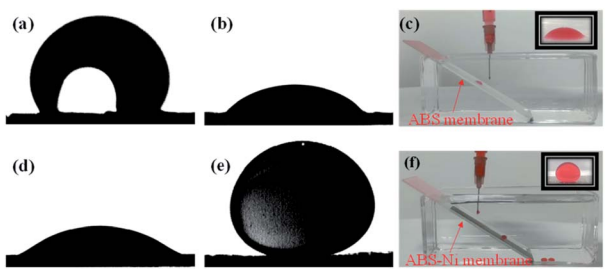

Fig. 5 WCA and UOCA of the prepared membranes: (a–c) ABS membrane; (d–f) ABS-Ni membrane.

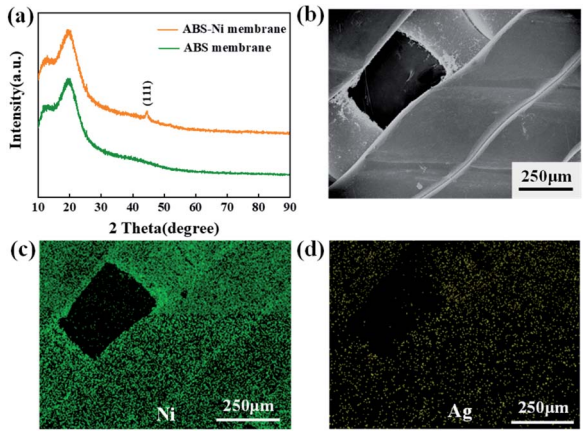

Fig. 6 (a) XRD and (b–d) EDS mapping images of the ABS-Ni membrane.

XPS was used to further analyze the composition of the ABS-Ni membrane. As shown in Fig. 7b, the two main peaks at 851.3 eV and 868.7 eV belong to Ni $2p_{3/2}$ and Ni $2p_{1/2}$, respectively. Meanwhile, the binding energy peaks of 854.7 eV and 872.4 eV are attributed to Ni^{2+}.[15,47] These results are well consistent with those shown in Fig. 6. Therefore, the success of coating an evenly distributed Ni layer is confirmed. Moreover, through the C 1s spectra (Fig. 7c and d), it can be seen that the content of C–OH groups in the ABS-Ni membrane increases, which indicates that the modification can endow the membrane surface with more hydroxyl groups. This is beneficial to improving the hydrophilicity of the membrane surface.[48–50]

3.3. Antifouling performance

The operating costs and practical ability depend on the antifouling performance of membranes. Fig. 8 clearly shows that

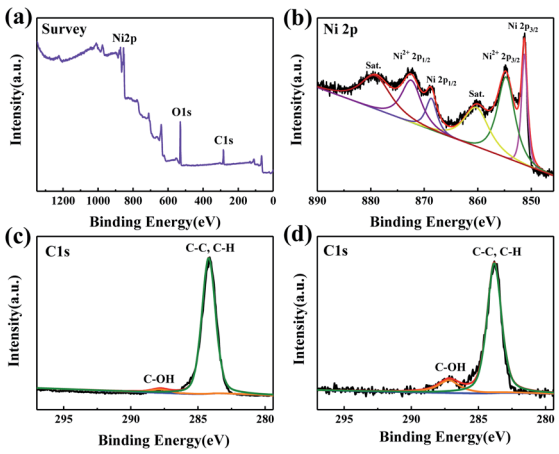

Fig. 7 (a, b) XPS patterns of the ABS-Ni membrane. (c, d) C 1s profile of the ABS and ABS-Ni membranes, respectively.

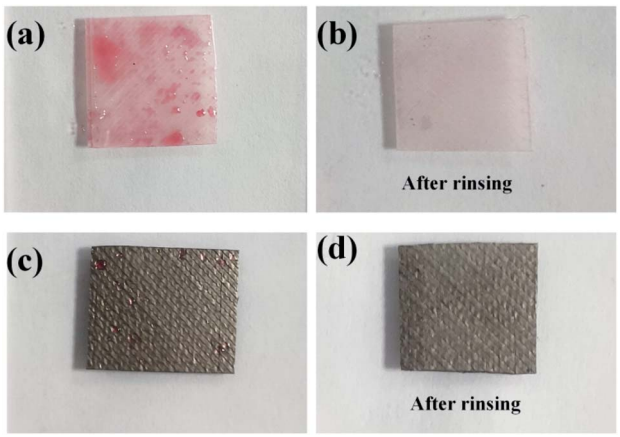

Fig. 8 Antifouling results of the (a, b) ABS and (c, d) ABS-Ni membranes.

the bare ABS membrane is seriously fouled by oil and cannot be totally cleaned by rinsing. Furthermore, the dynamic video tests shown in Fig. S2† reveal that the oil droplets directly adhere to the surface of the original membrane, while the oil drops cannot adhere onto the ABS-Ni membrane surface. Moreover, the dynamic contact tests reveal that the oil drops can freely roll down the ABS-Ni membrane surface. However, only a small amount of oil droplets are attached to the ABS-Ni membrane surface. Moreover, the membrane surface can be cleaned simply by rinsing. These results indicate that the ABS-Ni membrane has excellent antifouling ability for water/oil mixtures.

In order to explore the adhesion between oil and the membrane surface, the XDLVO theory was used to quantify the interface energy based on the data in Table 1. As shown in Fig. 9a, the total interaction energy between oil and the ABS membrane is negative, which indicates that oil adhesion is thermodynamically favorable.[51] In this case, the oil droplets can adhere to the membrane surface and cause membrane fouling. However, the total interaction energy between oil and the ABS-Ni membrane is positive, which indicates that the adhesion of oil to the ABS-Ni membrane is not thermodynamically favorable, which further proves that the ABS-Ni membrane has excellent antifouling performance.[52]

3.4. Oil/water separation performance

As shown in Fig. 10, both oil and water can directly pass through the bare ABS membrane, which indicates that the ABS membrane has low rejection ability for oil, while the ABS-Ni

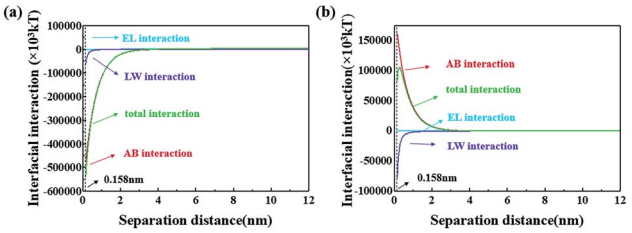

Fig. 9 Interaction energies at the interfaces of the (a) ABS and (b) ABS-Ni membranes.

membrane is able to quickly permeate the water and reject oil under the action of gravity. The videos in the ESI† vividly show the rather excellent separation performance of the ABS-Ni membrane over the ABS one. These results might be due to the high underwater superoleophobicity of the ABS-Ni membrane.

Fig. 11a shows the separation efficiency of the ABS-Ni membrane for the *n*-hexane, soybean oil, gasoline, diesel and petroleum ether systems. It can be seen that the ABS-Ni membrane displays more than 99% rejection for all the five oil/water systems. Fig. 11b demonstrates that the membrane has excellent antifouling performance through a cyclic filtration experiment. After 10 filtration cycles, the ABS-Ni membrane

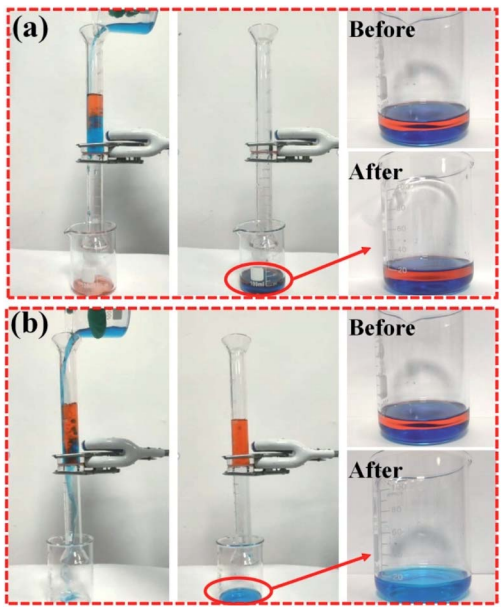

Fig. 10 Oil/water separation performance of the (a) ABS and (b) ABS-Ni membranes.

Table 1 Physicochemical parameters of the ABS and ABS-Ni membranes

Membrane	Contact angle (°)			Surface tensions (mJ m^{-2})			Zeta potential (mV)
	Ultrapure water	Glycerol	Diiodomethane	γ^{LW}	γ^{+}	γ^{-}	
ABS	96.87 ± 0.48	73.24 ± 0.97	27.09 ± 0.75	50.80	40.15	172.75	−47.53 ± 0.66
ABS-Ni	30.84 ± 1.19	112.97 ± 0.64	0	45.38	0.094	9.27	−16.85 ± 0.55

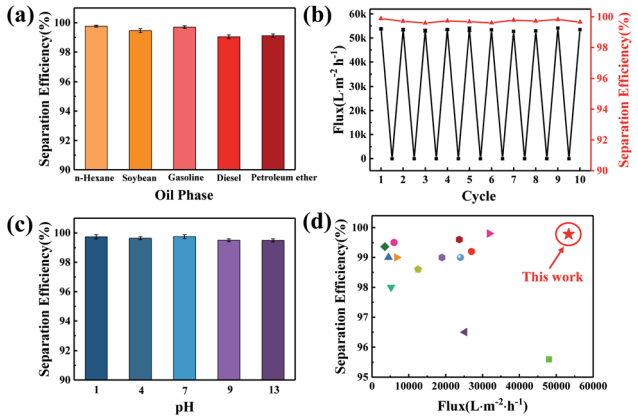

Fig. 11 Oil/water separation performance of the ABS-Ni membrane: (a) separation efficiency for different five oil/water systems; (b) separation efficiency in 10 cycles; (c) separation efficiency under different pH values; (d) comparison of separation efficiency.

retained a recovery flux ratio of above 99.5%, which is greatly superior in comparison with that from previous reports, as shown in Table S1.† Besides, Fig. 11c reveals that the ABS-Ni membrane retains stable separation functionality in the pH range from 1 to 13, indicating the extensive applicability of the fabricated membranes. These experimental results well prove that the ABS-Ni membrane has good antifouling performance and sustainable utilization ability. The oil/water separation performances of various membranes reported in the literature are summarized and compared, and the results are presented in Fig. 11d and the ESI (Table. S1†). Interestingly, it is found that the current ABS-Ni membrane outperforms all of the state-of-the-art membranes in terms of oil/water separation, to the best of our knowledge. Specifically, the flux and the rejection of the modified membrane for oil/water separation are extremely high, which is due to the favorable large pore size, surface roughness and improved hydrophilicity of the modified membrane, well breaking through the trade-off effect between permeability and rejection. Herein, the favorable membrane surface roughness refers to the roughness range beneficial to membrane flux improvement. The improved flux should be partly attributed to the fact that the modified membrane surface possesses preferential surface tension (γ^{LW}, γ^{+}, γ^{-}) and AB interaction energy, as analyzed by the XDLVO theory (Table 1 and Fig. 9). Fabricating membranes with extremely high permeance as well as high separation efficiency is an eternal pursuit of the research community. The exciting performance of the ABS-Ni membrane vividly shows that this goal can be achieved using the fabrication strategy proposed in this study. It is therefore argued that the ABS-Ni membrane can act as an excellent candidate for oil/water separation. The membrane fabrication strategy proposed by this work also gives important insights into membrane fabrication and oily wastewater treatment.

4. Conclusion

In this study, an ABS-Ni membrane was firstly prepared by 3D printing technology and applied for oil/water separation. The prepared ABS-Ni membrane exhibited underwater superoleophobicity, which was verified by its contact angle of 151.96°. The experimental results show that the ABS-Ni membrane possessed > 99% oil rejection to 5 kinds of oil/water systems namely *n*-hexane, soybean oil, gasoline, diesel and petroleum ether. Meanwhile, the flux of the ABS-Ni membrane reached as high as 5.34×10^4 L m^{-2} h^{-1}, which had an obvious superiority over the results in the literature. Moreover, both the flux and separation efficiency retained over 99% after 10 cycling filtration processes. Besides, the ABS-Ni membrane maintained stable separation functionality in the pH range from 1 to 13. These experimental results indicate that the ABS-Ni membrane can be an excellent candidate for oil/water separation.

Conflicts of interest

There are no conflicts to declare.

Acknowledgements

This study was financially supported by the Zhejiang Outstanding Youth Fund (No. LR22E080007), National Natural Science Foundation of China (Nos. 52070170, 51978628), Key Research and Development Program of Zhejiang Province (No. 2022C03069) and Zhejiang Provincial Ten Thousand Talent Program (ZJWR0302055).

References

1 S. Yuan, D. Strobbe, J.-P. Kruth, P. Van Puyvelde and B. Van der Bruggen, *J. Mater. Chem. A*, 2017, **5**, 25401–25409.
2 T. Ahmad, C. Guria and A. Mandal, *J. Water Proc. Eng.*, 2020, **36**, 1–14.
3 L. A. Mokif, H. K. Jasim and N. A. Abdlhusain, *Mater. Today: Proc.*, 2021, **49**, 2671–2674.
4 J.-J. Li, Y.-N. Zhou and Z.-H. Luo, *Prog. Polym. Sci.*, 2018, **87**, 1–33.
5 S. Schacht, Q. Huo, I. G. Voigt-Martin, G. D. Stucky and F. Schüth, *Science*, 1996, **273**, 768–771.
6 A. Almojjly, D. Johnson, D. L. Oatley-Radcliffe and N. Hilal, *J. Water Proc. Eng.*, 2018, **26**, 17–27.
7 J. Saththasivam, K. Loganathan and S. Sarp, *Chemosphere*, 2016, **144**, 671–680.
8 H. Wang, E. Wang, Z. Liu, D. Gao, R. Yuan, L. Sun and Y. Zhu, *J. Mater. Chem. A*, 2015, **3**, 266–273.
9 R. Li, J. Li, L. Rao, H. Lin, L. Shen, Y. Xu, J. Chen and B.-Q. Liao, *J. Membr. Sci.*, 2021, **619**, 118790.
10 M. Padaki, R. Surya Murali, M. S. Abdullah, N. Misdan, A. Moslehyani, M. A. Kassim, N. Hilal and A. F. Ismail, *Desalination*, 2015, **357**, 197–207.
11 M. M. Tao, L. X. Xue, F. Liu and L. Jiang, *Adv. Mater.*, 2014, **26**, 2943–2948.
12 L. H. Rao, X. J. You, B. H. Chen, L. G. Shen, Y. C. Xu, M. J. Zhang, H. C. Hong, R. J. Li and H. J. Lin, *Chemosphere*, 2022, 288.
13 F. Zhang, S. Gao, Y. Zhu and J. Jin, *J. Membr. Sci.*, 2016, **513**, 67–73.

14 B. S. Lalia, V. Kochkodan, R. Hashaikeh and N. Hilal, *Desalination*, 2013, **326**, 77–95.
15 A. Xie, J. Cui, J. Yang, C. Li, Y. Wang and J. Dai, *Appl. Clay Sci.*, 2021, **211**, 106161.
16 E. Tummons, Q. Han, H. J. Tanudjaja, C. A. Hejase, J. W. Chew and V. V. Tarabara, *Sep. Purif. Technol.*, 2020, **248**, 116919.
17 H. B. Park, J. Kamcev, L. M. Robeson, M. Elimelech and B. D. Freeman, *Science*, 2017, 356.
18 W. Wang, X. Du, H. Vahabi, S. Zhao, Y. Yin, A. K. Kota and T. Tong, *Nat. Commun.*, 2019, **10**, 3220.
19 A. Soo, S. M. Ali and H. K. Shon, *Desalination*, 2021, **520**, 115366.
20 A. Grant, B. Regez, S. Kocak, J. D. Huber and A. Mooers, *Results Mater.*, 2021, **12**, 100227.
21 K. Chawla, R. Singh and J. Singh, *Mater. Today: Proc.*, 2022, **48**, 1346–1351.
22 V. Harshitha and S. Srinivasa Rao, *Mater. Today: Proc.*, 2019, **19**, 583–588.
23 R. D. Farahani, M. Dubé and D. Therriault, *Adv. Mater.*, 2016, **28**, 5794–5821.
24 A. Siddiqui, N. Farhat, S. S. Bucs, R. V. Linares, C. Picioreanu, J. C. Kruithof, M. C. M. van Loosdrecht, J. Kidwell and J. S. Vrouwenvelder, *Water Res.*, 2016, **91**, 55–67.
25 N. Sreedhar, N. Thomas, O. Al-Ketan, R. Rowshan, H. Hernandez, R. K. Abu Al-Rub and H. A. Arafat, *Desalination*, 2018, **425**, 12–21.
26 T. Luelf, D. Rall, D. Wypysek, M. Wiese, T. Femmer, C. Bremer, J. U. Michaelis and M. Wessling, *J. Membr. Sci.*, 2018, **555**, 7–19.
27 S. Armbruster, A. Brochard, J. Lölsberg, S. Yüce and M. Wessling, *J. Membr. Sci.*, 2019, **570–571**, 537–546.
28 S. S. Ray, H. Dommati, J.-C. Wang and S.-S. Chen, *Ceram. Int.*, 2020, **46**, 12480–12488.
29 T. Femmer, A. J. C. Kuehne, J. Torres-Rendon, A. Walther and M. Wessling, *J. Membr. Sci.*, 2015, **478**, 12–18.
30 A. Al-Shimmery, S. Mazinani, J. Ji, Y. M. J. Chew and D. Mattia, *J. Membr. Sci.*, 2019, **574**, 76–85.
31 Y.-T. Chiou, M.-L. Hsieh and H.-H. Yeh, *Desalination*, 2010, **250**, 648–652.
32 H. Lin, M. Zhang, F. Wang, F. Meng, B.-Q. Liao, H. Hong, J. Chen and W. Gao, *J. Membr. Sci.*, 2014, **460**, 110–125.
33 W. Yu, Y. Liu, Y. Xu, R. Li, J. Chen, B.-Q. Liao, L. Shen and H. Lin, *J. Membr. Sci.*, 2019, **581**, 401–412.
34 Y. Liu, L. Shen, Z. Huang, J. Liu, Y. Xu, R. Li, M. Zhang, H. Hong and H. Lin, *J. Membr. Sci.*, 2022, **641**, 119925.
35 S. Xu, J. Li, Q. Ye, L. Shen and H. Lin, *J. Colloid Interface Sci.*, 2021, **589**, 525–531.
36 Z. Huang, Q. Zeng, Y. Liu, Y. Xu, R. Li, H. Hong, L. Shen and H. Lin, *J. Membr. Sci.*, 2021, **640**, 119854.
37 S. Xu, Y. Han, C. Zhou, J. Li, L. Shen and H. Lin, *Chin. Chem. Lett.*, 2022, 10265–10274.
38 F. Zhang, W. B. Zhang, Z. Shi, D. Wang, J. Jin and L. Jiang, *Adv. Mater.*, 2013, **25**, 4192–4198.
39 Z. Shi, W. B. Zhang, F. Zhang, X. Liu, D. Wang, J. Jin and L. Jiang, *Adv. Mater.*, 2013, **25**, 2422–2427.
40 T. Lin, Z. Lu and W. Chen, *J. Membr. Sci.*, 2014, **461**, 49–58.
41 D.-Q. He, L.-F. Wang, H. Jiang and H.-Q. Yu, *Chem. Eng. J.*, 2015, **272**, 128–134.
42 J. Liu, Y. Fan, Y. Sun, Z. Wang, D. Zhao, T. Li, B. Dong and C. Y. Tang, *J. Membr. Sci.*, 2021, **623**, 119048.
43 Z. Huang, J. Liu, Y. Liu, Y. Xu, R. Li, H. Hong, L. Shen, H. Lin and B.-Q. Liao, *J. Membr. Sci.*, 2021, 623.
44 J. Liu, L. Shen, H. Lin, Z. Huang, H. Hong and C. Chen, *J. Colloid Interface Sci.*, 2022, **618**, 483–495.
45 D.-H. Kang, J.-C. Choi, J.-M. Choi and T.-W. Kim, *Trans. Electr. Electron. Mater.*, 2010, **11**, 174–177.
46 X. Tang, C. Bi, C. Han and B. Zhang, *Mater. Lett.*, 2009, **63**, 840–842.
47 Q. Zeng, Y. Liu, L. Shen, H. Lin, W. Yu, Y. Xu, R. Li and L. Huang, *J. Colloid Interface Sci.*, 2021, **582**, 291–300.
48 J. Abenojar, R. Torregrosa-Coque, M. A. Martínez and J. M. Martín-Martínez, *Surf. Coat. Technol.*, 2009, **203**, 2173–2180.
49 Y. Kusano, H. Mortensen, B. Stenum, S. Goutianos, S. Mitra, A. Ghanbari-Siahkali, P. Kingshott, B. F. Sørensen and H. Bindslev, *Int. J. Adhes. Adhes.*, 2007, **27**, 402–408.
50 W. Zhao, Q. Ma, L. Li, X. Li and Z. Wang, *J. Adhes. Sci. Technol.*, 2013, **28**, 499–511.
51 R. Li, Y. Lou, Y. Xu, G. Ma, B.-Q. Liao, L. Shen and H. Lin, *Chemosphere*, 2019, **233**, 373–380.
52 L. G. Shen, Q. Lei, J. R. Chen, H. C. Hong, Y. M. He and H. J. Lin, *Chem. Eng. J.*, 2015, **269**, 328–334.